Journal of Applied Physics

RESEARCH ARTICLE | JANUARY 19 2011

# Sellmeier and thermo-optic dispersion formulas for $CsTiOAsO_4$

Takuya Mikami; Takayuki Okamoto; Kiyoshi Kato



*Journal of Applied Physics* 109, 023108 (2011)
https://doi.org/10.1063/1.3525800









AIP Publishing

# Sellmeier and thermo-optic dispersion formulas for $CsTiOAsO_4$

Takuya Mikami,[1,2,a] Takayuki Okamoto,[2] and Kiyoshi Kato[1]
[1]*Chitose Institute of Science and Technology, Bibi 758-65, Chitose, Hokkaido 066-8655, Japan*
[2]*Okamoto Optics Work, Inc., Haramachi 8-34, Isogo-ku, Yokohama, Kanagawa 235-0008, Japan*

(Received 13 September 2010; accepted 10 November 2010; published online 19 January 2011)

$CsTiOAsO_4$ has been found to be phase-matchable for type-2 second-harmonic generation and sum-frequency generation in the 0.5321–1.5915 $\mu$m range at 20.0 °C. The Sellmeier equations that correctly reproduce these experimental data as well as the 90° phase-matched optical parametric oscillator wavelengths in the 0.7337–2.4793 $\mu$m range are presented together with the thermo-optic dispersion formula. © *2011 American Institute of Physics*. [doi:10.1063/1.3525800]

## I. INTRODUCTION

Although the optical parametric oscillation (OPO) in $CsTiOAsO_4$ (CTA) has been reported by several authors,[1–3] somewhat large discrepancies between theory and experiment were encountered for the Nd:YAG laser excitation.[2] In order to check the validity of the Sellmeier equations of Cheng *et al.*[4] and Feve *et al.*,[5] we have remeasured the type-2 OPO wavelengths by pumping the 2 cm long, x-cut CTA crystal grown by a flux method (supplied earlier by Crystal Associates Inc.)[6] with the Nd:YAG laser at 1.0642 $\mu$m and its second harmonic generation (SHG) at 20.0 °C. The generated signal and idler wavelengths were $\lambda_s=1.8645$ and $\lambda_i=2.4793$ $\mu$m under the Nd:YAG laser excitation, and $\lambda_s=0.7337$ and $\lambda_i=1.9365$ $\mu$m under the SHG excitation. In addition, we have found that this crystal is 90° phase-matchable for type-2 SHG of the Nd:YAG laser-pumped $KTiOPO_4$ (KTP)/OPO at 1.2836 and 3.1830 $\mu$m along y axis. These results except the short SHG cutoff wavelength calculated with the Sellmeier equations of Cheng *et al.*[4] are significantly different from the values given by those of Cheng *et al.*[4] and Feve *et al.*[5]

Thus, we have constructed the new Sellmeier equations that provide a good reproduction of our new experimental results for OPO, and type-2 SHG, and sum-frequency generation (SFG) in the 0.5321–1.5915 $\mu$m range. In addition, since no data is available for the thermo-optic constants for this material in the literature, we measured these parameters and have constructed the dispersion formula that provides a good reproduction of our experimental data for the temperature-dependent phase-matching conditions for type-2 SHG and SFG in the 0.5321–0.7778 $\mu$m range.

## II. EXPERIMENTS AND DISCUSSION

By using the refractive indices in the visible given by the Sellmeier equations of Cheng *et al.*,[4] we have adjusted the Sellmeier constants in the IR to give the best fit to the above-mentioned OPO and SHG data as well as SFG data tabulated in Table I. The newly constructed Sellmeier equations are expressed as

$$n_x^2 = 1.91529 + \frac{1.47442\lambda^2}{\lambda^2 - 0.03636} + \frac{3.34240\lambda^2}{\lambda^2 - 256.3489},$$

$$n_y^2 = 2.17626 + \frac{1.25709\lambda^2}{\lambda^2 - 0.04516} + \frac{3.57582\lambda^2}{\lambda^2 - 268.5551},$$

$$n_z^2 = 2.46519 + \frac{1.16730\lambda^2}{\lambda^2 - 0.06049} + \frac{3.69079\lambda^2}{\lambda^2 - 278.8889},$$

$$(0.5321\ \mu\text{m} \le \lambda \le 3.183\ \mu\text{m}), \quad (1)$$

where $\lambda$ is in micrometers.

In order to check the validity of these equations, we have calculated the phase-matching angles for type-2 SHG in the x-y ($\theta=90°$) and y-z ($\phi=90°$) planes for the short and long wavelength range. The results are shown in Figs. 1 and 2 together with the tuning curves calculated with the Sellmeier equations of Cheng *et al.*[4] and Feve *et al.*[5] As can be seen from these figures, the SHG data points of Feve *et al.*[5] in the short wavelength range differ significantly from our experimental points. For instance, the phase-matching angles for SHG at 0.6594 $\mu$m calculated with our Sellmeier equations of ($\theta=77.4°$, $\phi=90°$) and ($\theta=90°$, $\phi=66.2°$) agree well with the values of ($\theta=76.0°$, $\phi=90°$) and ($\theta=90°$, $\phi=64.3°$) given by Cheng *et al.*[4,7] but differ significantly from Feve *et al.*'s theoretical values of ($\theta=73.7°$, $\phi=90°$) and ($\theta=90°$, $\phi=62.1°$),[5] and Boulanger *et al.*'s[8] data of ($\theta=73.1°$, $\phi=90°$) and ($\theta=90°$, $\phi=59.0°$). Nevertheless, the acceptance angles [full width at half maximum (FWHM)] of $\Delta\theta_{ext}\cdot\ell=8.8$ mrad cm in the y-z plane and $\Delta\phi_{ext}\cdot\ell=16.9$ mrad cm in the x-y plane given by Boulanger *et al.*[8] agree fairly well with our calculated values of $\Delta\theta_{ext}\cdot\ell=9.0$ mrad cm and $\Delta\phi_{ext}\cdot\ell=17.9$ mrad cm, respectively. While Cheng *et al.*'s[4] value is $\Delta\phi_{int}\cdot\ell \cong 8.6$ mrad cm at ($\theta=90°$, $\phi=64.3°$). However, Feve *et al.*'s index formula[5] gives the angular acceptance of $\Delta\theta_{ext}\cdot\ell=6.1$ mrad cm in the y-z plane and $\Delta\phi_{ext}\cdot\ell=10.9$ mrad cm in the x-y plane, which differ significantly from the values measured by Boulanger *et al.*[8] using the same sample. These inconsistencies may be attributed to the local variation in the refractive index of their crystal, or the inaccuracy in the Sellmeier equations.

[a]Electronic mail: mikami@okamoto-optics.co.jp.

 

TABLE I. Phase-matching conditions for type-2 OPO, SHG, and SFG in CTA. Note: $1/\lambda_1+1/\lambda_2=1/\lambda_3$. The superscripts of the interacting wavelengths represent the polarization directions.

| | Wavelength ($\mu$m) | | | Phase-matching loci ($\theta, \phi$) | | | |
|---|---|---|---|---|---|---|---|
| | | | | Calculated | | | |
| | $\lambda_1$ | $\lambda_2$ | $\lambda_3$ | Cheng *et al.* | Feve *et al.* | Mikami *et al.* | Measured |
| SHG | $1.2836^{x}$ | $1.2836^{z}$ | $0.6418^{x}$ | (85.5°, 90°) | (80.4°, 90°) | (90°, 90°) | (90°, 90°) |
| | $1.3188^{x}$ | $1.3188^{yz}$ | $0.6594^{x}$ | (76.4, 90) | (73.7, 90) | (77.4, 90) | (77.4, 90) |
| | | | | | | | (76.0, 90)[a] |
| | | | | | | | (73.1, 90)[b] |
| | $1.3188^{xy}$ | $1.3188^{z}$ | $0.6594^{xy}$ | (90, 63.1) | (90, 62.3) | (90, 66.2) | (90, 66.2) |
| | | | | | | | (90, 64.3)[c] |
| | | | | | | | (90, 64.0)[a] |
| | | | | | | | (90, 59.0)[b] |
| | $1.5556^{y}$ | $1.5556^{z}$ | $0.7778^{y}$ | (86.6, 0) | (90, 10.8) | (90, 0) | (90, 0) |
| | $3.183^{x}$ | $3.183^{z}$ | $1.5915^{x}$ | ⋯ | ⋯ | (90, 90) | (90, 90) |
| SFG | $1.3408^{x}$ | $1.0642^{z}$ | $0.5933^{x}$ | (85.0, 90) | (80.9, 90) | (90, 90) | (90, 90) |
| | $1.8645^{y}$ | $1.0642^{xz}$ | $0.6775^{y}$ | (70.7, 0) | (73.8, 0) | (72.5, 0) | (72.4, 0) |
| | $1.4437^{x}$ | $0.8427^{z}$ | $0.5321^{x}$ | ⋯ | (81.6, 90) | (90, 90) | (90, 90) |
| | $1.9059^{xy}$ | $0.7382^{z}$ | $0.5321^{xy}$ | (84.3, 0) | (90, 24.5) | (90, 13.0) | (90, 13.0) |
| | $2.023^{y}$ | $0.722^{xz}$ | $0.5321^{y}$ | (77.0, 0) | (90, 8.0) | (79.8, 0) | (80.2, 0) |
| OPO | $2.4793^{z}$ | $1.8645^{y}$ | $1.0642^{y}$ | (90, 37.2) | (90, 17.8) | (90, 0) | (90, 0) |
| | $1.9365^{y}$ | $0.7337^{z}$ | $0.5321^{y}$ | (81.7, 0) | (90, 21.1) | (90, 0) | (90, 0) |

[a]Reference 7.
[b]Reference 8.
[c]Reference 4.

In the long wavelength range, there are no experimental data thus far published in the literature. However, we note that our measured and calculated SHG cutoff wavelength of 1.5915 $\mu$m is significantly different from the theoretical values of $\lambda_2=1.4734$ $\mu$m and 1.5498 $\mu$m given by the index formulas of Cheng *et al.*[4] and Feve *et al.*,[5] respectively.

We next have computed the 90° phase-matched OPO wavelengths in the x-cut crystal. Plotted in Fig. 3 are the data points given by Powers *et al.*,[1] Rines *et al.*,[2] and the present authors. The dashed lines (C), dotted lines (F), and real lines (M) are the theoretical curves calculated with the Sellmeier equations of Cheng *et al.*,[4] Feve *et al.*,[5] and the present authors, respectively. As shown in this figure, the phase-matching curves calculated with our index formula give the best fit to these experimental points.

However, for the critical phase-matching, we were unable to fit the experimental points at wavelengths longer than 4 $\mu$m for the type-2 different-frequency generation (DFG) between the near-IR OPO and the Nd:YAG laser given by Feve *et al.*[5] Our calculated values at 4 $\mu$m are about 3.5° and 5° larger than their experimental values in the x-z and y-z planes, respectively.

Similar deviation from the experimental points has been obtained when using the Sellmeier equations of Cheng *et al.*[4]

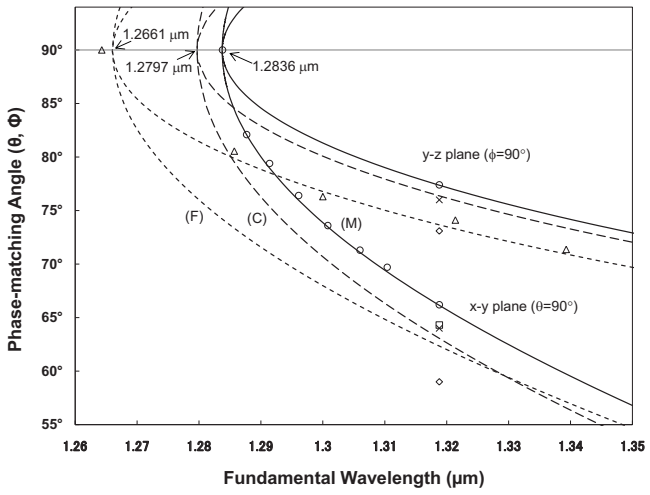


FIG. 1. Phase-matching curves for type-2 SHG in CTA in the short wavelength branch. The square, triangle, cross, lozenge, and circle points are the experimental data taken from Refs. 4, 5, 7, and 8, and our data, respectively. The dashed lines (C), dotted lines (F), and real lines (M) are calculated with the index formulas of Cheng *et al.* (Ref. 4), Feve *et al.* (Ref. 5), and the present authors, respectively.

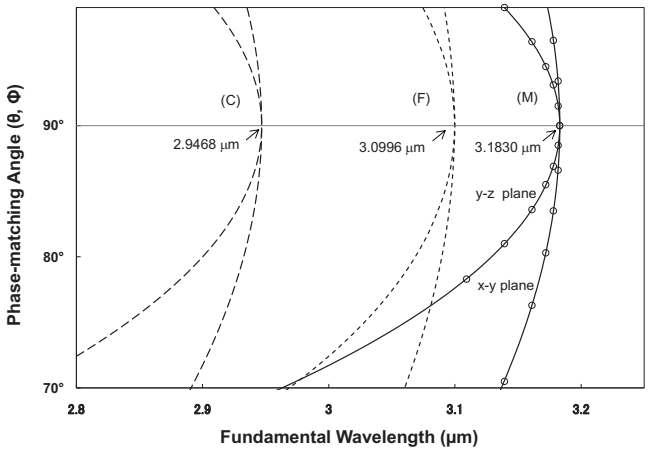


FIG. 2. Phase-matching curves for type-2 SHG in CTA in the long wavelength branch. The circle points are our experimental points. The dashed lines (C), dotted lines (F), and real lines (M) are calculated with the index formulas of Cheng *et al.* (Ref. 4), Feve *et al.* (Ref. 5), and the present authors, respectively.

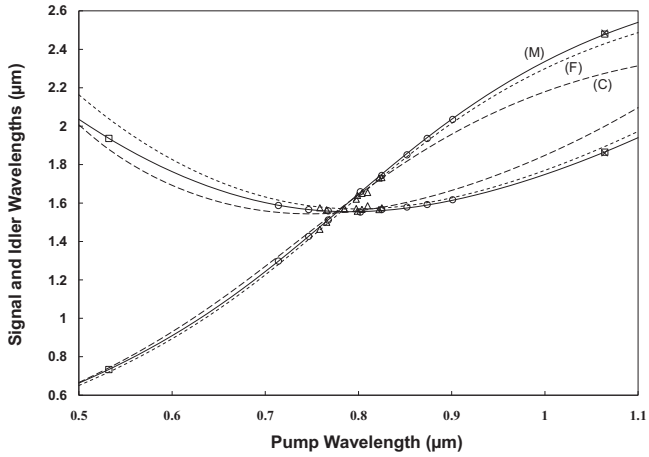


FIG. 3. 90° phase-matching curves for CTA OPO along x-axis. The triangle, circle, cross, and square points are the experimental points taken from Refs. 1 and 2, and the present authors, respectively. The dashed lines (C), dotted lines (F), and real lines (M) are the theoretical curves calculated with the index formulas of Cheng *et al.*(Ref. 4), Feve *et al.*(Ref. 5), and the present authors, respectively.

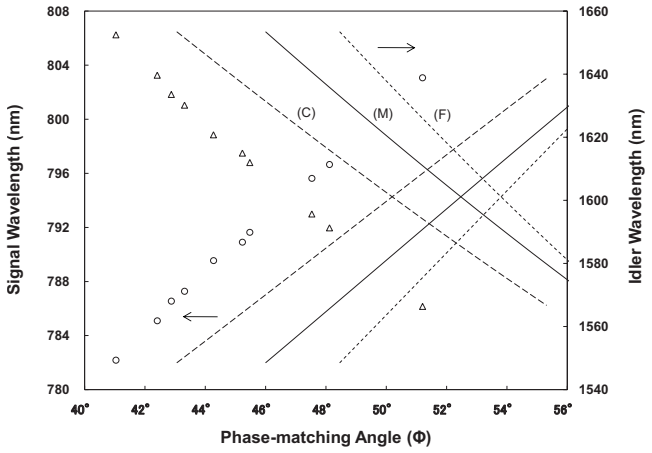


FIG. 4. Phase-matching curves for type-2 DFG in the x-y plane in CTA between the Kr-ion laser at 0.5309 $\mu$m and the tunable Ti:sapphire laser. The circle and triangle points are the input signal and output idler wavelengths that are taken from Ref. 11. The dashed lines (C), dotted lines (F), and real lines (M) are the theoretical curves calculated with the index formulas of Cheng *et al.* (Ref. 4), Feve *et al.*(Ref. 5), and the present authors, respectively.

These results strongly suggest that their crystal has significantly different refractive indices in the IR from ours. Indeed, their Sellmeier equations constructed to fit these experimental points give $n_z < n_y, n_x$ at wavelengths longer than ~4.5 $\mu$m, which contrasts sharply with our Sellmeier equations having a normal dispersion $n_z > n_y > n_x$ in the whole spectral range. Despite this discrepancy encountered in CTA, their experimental points for $KTiOAsO_4$ and $RbTiOAsO_4$ agree well with the values calculated with our Sellmeier equations.[9,10]

We have also computed the phase-matching angles for type-2 DFG between the Kr-ion laser at 0.5309 $\mu$m and the tunable Ti:sapphire laser in the x-y plane. Figure 4 shows the tuning curves calculated with the Sellmeier equations of Cheng *et al.*,[4] Feve *et al.*,[5] and the present authors. Our tuning curves are 5°–6° larger than the experimental points given by Lai *et al.*[11] and fall between the curves (C) and (F). The discrepancy between theory and experiment is probably due to the crystal to crystal variation in the refractive indices and the possible error in our Sellmeier constants, although we cannot rule out the small variation in the phase-matching angle caused by the local heating of the crystal owing to its high absorption at 0.5309 $\mu$m.[11]

In order to predict precisely the temperature-dependent phase-matching conditions for this material, we measured the thermo-optic constants $dn_x/dT$, $dn_y/dT$, and $dn_z/dT$ from 20 to 120 °C at temperature intervals of 20 °C with the minimum deviation method in the 0.532–1.571 $\mu$m range. Two right triangle prisms used in this experiment were cut from the same sample that was used for the OPO experiments, and fabricated at apex angles of 30.09° and 29.91° in the x-y plane with the light incident surface being normal to

TABLE II. Temperature phase-matching bandwidths (FWHM) for type-2 SHG and SFG in CTA. Note: $1/\lambda_1+1/\lambda_2=1/\lambda_3$. The superscripts of the interacting wavelengths represent the polarization directions.

| | Wavelength ($\mu$m) | | | Phase-matching loci ($\theta, \phi$) | | | $\Delta T \cdot \ell$ (°C cm) | |
|---|---|---|---|---|---|---|---|---|
| | $\lambda_1$ | $\lambda_2$ | $\lambda_3$ | Measured | Calculated | Angular acceptance | Measured | Calculated |
| SHG | $1.2836^x$ | $1.2836^z$ | $0.6418^x$ | (90°, 90°) | (90°, 90°) | $\Delta\theta_{ext} \cdot \ell^{1/2}=4.8$<br>$\Delta\phi_{ext} \cdot \ell^{1/2}=8.8$<br>(deg cm$^{1/2}$) | 8.4[a] | 8.5 |
| | $1.3188^x$ | $1.3188^{yz}$ | $0.6594^x$ | (77.4, 90) | (77.4, 90) | $\Delta\theta_{ext} \cdot \ell=9.0$ (mrad cm) | 8.9 | 8.9 |
| | $1.3188^{xy}$ | $1.3188^z$ | $0.6594^{xy}$ | (90, 66.2) | (90, 66.2) | $\Delta\phi_{ext} \cdot \ell=17.9$ (mrad cm) | 9.0 | 8.9 |
| | $1.5556^y$ | $1.5556^z$ | $0.7778^y$ | (90, 0) | (90, 0) | $\Delta\theta_{ext} \cdot \ell^{1/2}=4.8$<br>$\Delta\phi_{ext} \cdot \ell^{1/2}=10.3$<br>(deg cm$^{1/2}$) | 11.1[a] | 10.4 |
| SFG | $1.3408^x$ | $1.0642^z$ | $0.5933^x$ | (90, 90) | (90, 90) | $\Delta\theta_{ext} \cdot \ell^{1/2}=4.3$<br>$\Delta\phi_{ext} \cdot \ell^{1/2}=7.9$<br>(deg cm$^{1/2}$) | 7.5[a] | 7.5 |
| | $1.9059^{xy}$ | $0.7382^z$ | $0.5321^{xy}$ | (90, 13.0) | (90, 13.0) | $\Delta\phi_{ext} \cdot \ell=14.5$ (mrad cm) | 7.2 | 8.6 |
| | $2.023^y$ | $0.722^{xz}$ | $0.5321^y$ | (80.2, 0) | (79.8, 0) | $\Delta\theta_{ext} \cdot \ell=4.5$ (mrad cm) | 11.1 | 8.6 |

[a]Measured by $d\lambda_1/dT$.

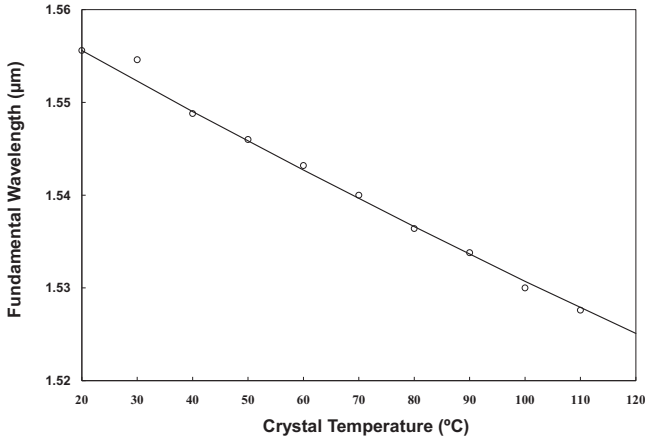


FIG. 5. Temperature-tuned 90° phase-matching curve for type-2 SHG along x axis. The pump source is the Nd:YAG laser-pumped KTP/OPO. The circle points are our experimental points. The real line is calculated with our index and thermo-optic dispersion formulas presented in Sec. II.

the x or y axis. The light sources used in this experiment were the He–Ne lasers, the Nd:YAG laser, and the Nd:YAG laser-pumped KTP/OPO.

These raw data were adjusted to give the best fit to the measured temperature phase-matching bandwidths (FWHM) for type-2 SHG and SFG (Table II), that were determined by the calculated angular acceptance ($\Delta\theta_{ext}\cdot\ell$) and the temperature variation in the phase-matching angle ($\Delta\theta_{pm}/\Delta T$), and the temperature-dependent phase-matching conditions for the 90° phase-matched SHG and SFG along x and y axes that are shown in Figs. 5 and 6. The circle points are our experimental points. The real lines are calculated with our Sellmeier equations coupled with the following thermo-optic dispersion formula given by:

$$\frac{dn_x}{dT} = \left(\frac{0.3436}{\lambda^3} - \frac{0.4197}{\lambda^2} + \frac{0.3161}{\lambda} + 0.8231\right) \times 10^{-5}, \quad (^\circ C^{-1}),$$

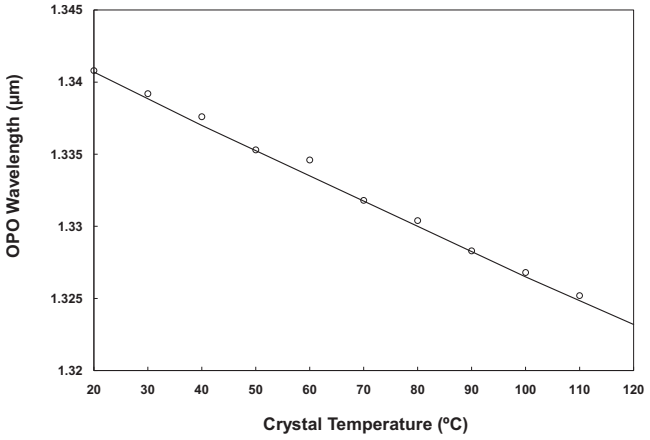


FIG. 6. Temperature-tuned 90° phase-matching curve for type-2 SFG along y axis. The pump source are the Nd:YAG laser and its SHG-pumped KTP/OPO. The circle points are our experimental points. The real line is calculated with our index and thermo-optic dispersion formulas presented in Sec. II.

$$\frac{dn_y}{dT} = \left(\frac{0.5958}{\lambda^3} - \frac{0.8120}{\lambda^2} + \frac{0.6376}{\lambda} + 0.8546\right) \times 10^{-5},$$

$$\frac{dn_z}{dT} = \left(\frac{1.5170}{\lambda^3} - \frac{2.7879}{\lambda^2} + \frac{2.5353}{\lambda} + 2.5586\right) \times 10^{-5},$$

$$(0.5321\ \mu m \le \lambda \le 2.023\ \mu m), \quad (2)$$

where λ is in micrometers.

Although no attempt was made to exclude the thermal expansion terms owing to the total lack of the thermal expansion coefficient, Eq. (2) reproduces well the temperature-dependent phase-matching conditions for type-2 SHG and SFG in the 0.5321–0.7778 μm range when coupled with our Sellmeier equations [Eq. (1)].

Meanwhile, we have attempted to construct the temperature dependent Sellmeier equations based on Eqs. (1) and (2). However, we were unable to derive the high-accuracy formula to reproduce well the temperature phase-matching bandwidths tabulated in Table II, and hence we have used independently Eqs. (1) and (2) for the present studies.

Since this compound is 90° phase-matchable for SHG at 0.775 μm along x by temperature tuning, it is highly useful for the SHG of the high-average power Er-doped fiber laser owing to its large temperature bandwidth $\Delta T\cdot\ell \cong 10$ °C cm, large nonlinear optical constant [$d_{32}(1.064\ \mu m) = 3.4 \pm 0.7$ pm/V],[4] and large acceptance angles ($\Delta\theta_{ext}\cdot\ell^{1/2} = 4.7$ deg $cm^{1/2}$ and $\Delta\phi_{ext}\cdot\ell^{1/2} = 10.1$ deg $cm^{1/2}$).

## III. CONCLUSION

We have reported the high accuracy Sellmeier and thermo-optic dispersion formulas that reproduce well the temperature-dependent phase-matching conditions for OPO, SHG in the 0.6419–0.7778 μm, and SFG in the 0.5321–0.5933 μm. We believe these equations would be highly useful for predicting the various frequency conversion systems based on CTA.

[1]P. E. Powers, C. L. Tang, and L. K. Cheng, Opt. Lett. **19**, 37 (1994).
[2]G. A. Rines, H. H. Zenzie, R. A. Schwarz, Y. Isyanova, and P. F. Moulton, IEEE J. Sel. Top. Quantum Electron. **1**, 50 (1995).
[3]G. R. Holtom, R. A. Crowell, and L. K. Cheng, Opt. Lett. **20**, 1880 (1995).
[4]L. T. Cheng, L. K. Cheng, J. D. Bierlein, and F. C. Zumsteg, Appl. Phys. Lett. **63**, 2618 (1993).
[5]J. P. Feve, B. Boulanger, O. Pacaud, I. Rousseau, B. Menaert, G. Marnier, P. Villeval, C. Bonnin, G. M. Loiacono, and D. N. Loiacono, J. Opt. Soc. Am. B **17**, 775 (2000).
[6]G. M. Loiacono, D. N. Loiacono, and R. A. Stolzenberger, J. Cryst. Growth **131**, 323 (1993).
[7]L. T. Cheng, L. K. Cheng, and J. D. Bierlein, Proc. SPIE **1863**, 43 (1993).
[8]B. Boulanger, J. P. Feve, G. Marnier, G. M. Loiacono, D. N. Loiacono, and C. Bonnin, IEEE J. Quantum Electron. **33**, 945 (1997).
[9]K. Kato and N. Umemura, Proceedings of the Laser and Electro-Optics/Quantum Electronics and Laser Science Conference, 2004, p. CThT35.
[10]K. Kato, E. Takaoka, and N. Umemura, Jpn. J. Appl. Phys., Part 1 **42**, 6420 (2003); The IR dispersion terms of $n_x$ and $n_y$ were improved. The new formula is expressed as: $n_x^2 = 2.04726 + 1.17229\lambda^2/(\lambda^2 - 0.04063) + 1.31785\lambda^2/(\lambda^2 - 131.0365)$, $n_y^2 = 2.12600 + 1.11562\lambda^2/(\lambda^2 - 0.04532) + 1.38410\lambda^2/(\lambda^2 - 134.0264)$, $n_z^2 = 2.19499 + 1.29498\lambda^2/(\lambda^2 - 0.05241) + 3.51232\lambda^2/(\lambda^2 - 261.3629)$.
[11]B. Lai, N. C. Wong, and L. K. Cheng, Opt. Lett. **20**, 1779 (1995).